

Highly Maneuverable Biorobotic Underwater Vehicles

Promode R. Bandyopadhyay

After receiving only a trickle of interest over the past 50 years or so, biolocomotion has more recently attracted broader attention. In this chapter, biology-inspired highly maneuverable underwater vehicles (of ≈ 1 m length scale) that have achieved some degree of maturity are reviewed. Primarily, the Naval Undersea Warfare Center (NUWC) works are described. The nonlinear theoretical foundation of animal-inspired hydrodynamics and control is summarized. Low-speed propulsion (including hovering and maneuvering), control, and integration with sensors are considered. High-lift flapping-fin propulsion technology, cycle-averaged and olivo-cerebellar temporal control, integration with interaural time-differencing bio-sonar, and basin demonstration of utility are discussed. While numerous variables affect the mechanisms and integration of actuators, controllers, and sensors, the principles of self-regulating nonlinear dynamics provide a common and simplifying framework for the development of biorobotic vehicles. The salient features of these vehicles and their control design laws are tabulated. These emergent, low-speed platforms complement existing higher speed naval capabilities and are not substitutes for any existing mature system; in this sense, their utility depends on the imaginative nature of future operation concepts – a process that is unpredictable. The greater potential of the biorobotics approach is limited by a serious lack of progress in so-called strong artificial muscle technology, as well as by a lack of understanding of nonlinear temporal control and

11.1	Biorobotics	281
11.1.1	Flapping Fin Propulsion Technology	284
11.2	Theoretical Foundation of Animal-Inspired Hydrodynamics and Control	286
11.2.1	Hydrodynamics	286
11.2.2	Animal-Like Motion Control Laws and the Principles of Integrated Design	287
11.3	Description of Biology-Inspired Vehicles of Emergent Maturity	289
11.4	Reliability, Low Power Consumption, and Disturbance Rejection of Bio-Inspired Propulsion	296
11.5	Demonstrated Maneuverings of NUWC Bio-Inspired Vehicles	296
11.5.1	BAUV	296
11.5.2	SPLINE	297
11.5.3	RAZOR	297
11.6	Discussion	297
11.7	Concluding Remarks	298
11.8	Nomenclature	298
	References	299

sensing and how they should be integrated. Application to utility has been facilitated where understanding of the underlying science has been mathematically formulated, and such formulation needs to be more widely emulated.

11.1 Biorobotics

The 1934 work of *Karman* and *Burgers* [11.1] laid the early theoretical foundation of biorobotics, followed in 1975 by *Lighthill* and others [11.2], who established a broader foundation. *Karman* and *Burgers* give the key insight into the hydrodynamic mechanism of biolocomotion [11.2, Fig. 8], which states that in a swimming

fish, caudal fins need to flap just enough to produce vortex wakes to give rise to a thrust jet, and the *Karman* vortex street is present in reverse. However, energy is not wasted in excessive flapping in making the vortex wake and yet the jet cross-section is large, whereby *good efficiency* is achieved [11.2, p. 30].

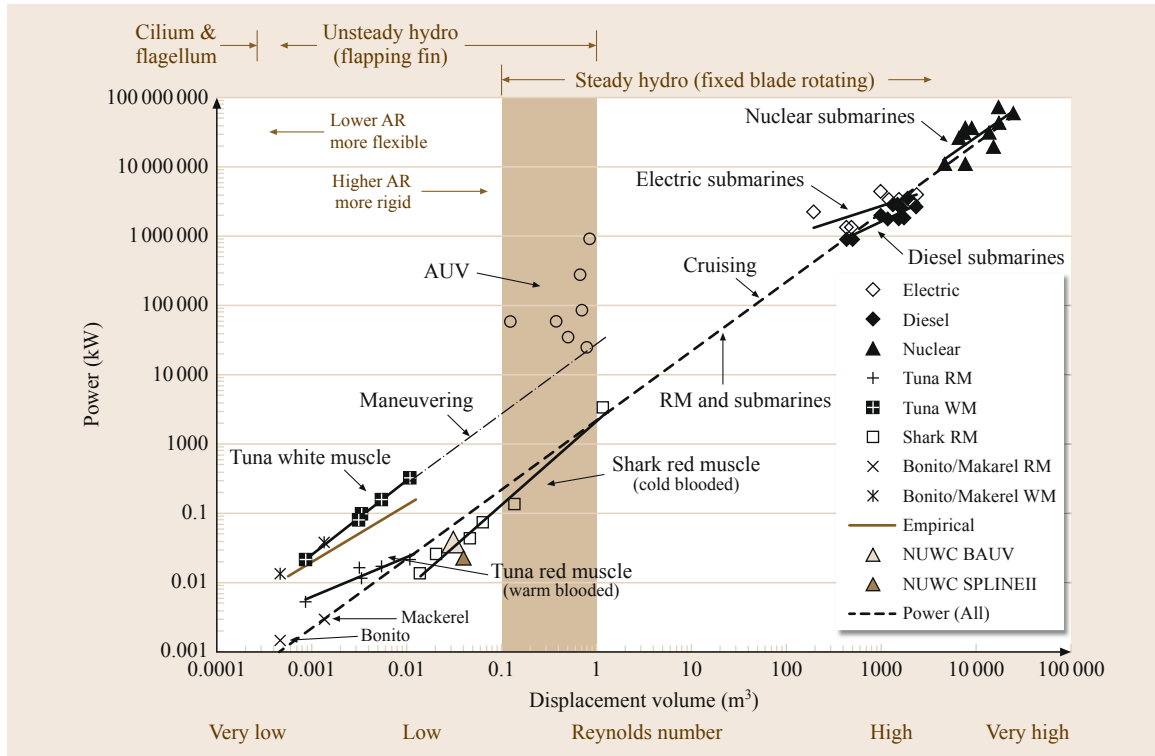


Fig. 11.1 Comparison of propulsion density of animal and manmade autonomous underwater swimmers; the latter shows both biorobotic vehicles (NUWC BAUV, and SPLINEII) and swimmers with conventional rotating propulsors. BAUV: biorobotic autonomous underwater vehicle; SPLINE: self-propelled line array; RM: red muscle (used for cruising); WM: white muscle (used for maneuvering, which follows a different trend (after [11.3])). For data source, see [11.3, 4]; the submarine data are from the open literature [11.5, 6] (reproduced after [11.4, Fig. 3] and after [11.3, Fig. 6])

Biocomotion is now seen as more than hydrodynamics because animals are seen to be perfectly autonomous, with excellent maneuvering and sensing abilities – a perfect *unmanned underwater vehicle* so to speak. Reverse engineering of swimming animals is thus seen as instructive and the subject of biorobotics attempts to find utility in those animal properties. Here we review the more mature progress in this field.

Research on bio-inspired underwater vehicles seeks to expand the operational envelope by implementing *integrated* principles of hydrodynamics, control, materials, and sensing. The integrated nature of these principles and the differences between bio-inspiration and bio-mimicry are important aspects that we need to understand because success hinges on that understanding. The measure of success is readiness for demonstration on real missions (*transitionability* in naval context) to practical value, and realization of the potential depends on the maturity achieved over a period of 5–10 years, during which a substantial amount of investment will have been made. These aspects are considered below.

We are aware that in ocean engineering, bio-inspired vehicles are considered by some practically minded, influential people as just a curiosity. To rebut such notions, the focus in this review is on vehicles of emergent maturity, as described below. We do not consider the numerous biorobotic vehicles that have not made it out of the confines of the small tank or laboratory, including some of our own early works. Thus, this review leans more on our US Navy work over the last decade, and on the open literature in regard to others' work.

Figure 11.1 shows a meta-analysis of propulsive power (kW) versus displacement volume (m^3), extending over eight decades of these two parameters, has been carried out for engineering underwater vehicles and for animals [11.3–6]. Data from the open literature were utilized. For the animals, the propulsive power was separated for cruising and maneuvering; these functions are attributed to red and white muscles, respectively. The trend for cruising was identical between the engineering vehicles and the red muscles indicating that the drag levels are minimized. The ani-

mals shown use flapping caudal and/or pectoral fins for propulsion/maneuvering. Since the propulsive mechanism of these flapping lifting surfaces makes use of transitional vortex shedding, it must be that larger and larger biorobotic vehicles can also be built with flapping fin propulsion as long as the fin Reynolds number is within the critical range. From the graph in Fig. 11.1, this is a limit of displacement volume of the order of 1 m^3 (of the size of a large shark). (We have not been able to find animal data between 2 and 100 m^3 , and a higher limit is not ruled out.) The tuna white muscle data shows that power required for maneuvering is 10 times greater than that required for cruising. Below, we review our biorobotic vehicles of displacement volume of the order of 0.05 m^3 .

Let us begin with several important definitions. A *mature platform based on bio-inspiration or bio-mimicry* is one for which:

1. A user mission has been identified.
2. An instrumented version has been built and demonstrated both in the laboratory and in open/saltwaters.
3. Integration with mission sensors has been demonstrated.
4. Documentation or knowledge about improvements over conventional engineering solutions and mechanisms have been experimentally verified and theoretically backed.
5. The biology principle, mechanism, and design laws have been determined, are mathematically founded, and have been peer reviewed, and
6. Long-duration performance has been demonstrated.

Bio-inspiration is described as an undertaking in which the science has been distilled and implemented in a framework that is useful to a user where a bio-inspired platform does not necessarily resemble any animal. In contrast, *bio-mimicry* is an effort in which, first and foremost, biology is mimicked and whereby the resulting platform resembles the chosen animal. The latter, which tends to draw popular interest, may have value in camouflaging.

The subject of unmanned biorobotic underwater vehicles has been reviewed in the past [11.7, 8]. The underlying science and technology have been reviewed by several authors [11.2–4, 7–17]. From the larger biorobotic point of view ($\approx 1 \text{ m}$ scale), we separate the propulsive surfaces of animal swimmers in two categories as follows: smaller swimmers with highly flexible caudal and pectoral fins and with main bodies that are more on the flexible side (they have lower Reynolds number); generally larger swimmers whose fins are rather rigid (but not fully rigid) with bodies that are more on the rigid side (they have higher Reynolds number) [11.13]. An example of the former

is sunfish (the kind of fish extensively studied in the laboratory [11.18]), and the examples of the latter are penguins, dolphins and whales (the fins are studied mostly biorobotically [11.3, 11, 14, 15, 19]). (Box fish with its rigid body and flexible fins straddles the two categories [11.20].)

Biorobotics received an early boost with the bio-mimicry of caudal fin swimming of tuna fish [11.21–23] in a similar flexible hull. This was followed by departure from bio-mimicry of form – by the application of flapping fin propulsion technology to rigid cylinders – the common engineering underwater hull forms of choice [11.19]. This chapter focuses mainly on flapping fin propulsion and control technology, and the fins are large and fairly stiff (or only slightly flexible).

In relation to swimming animals and from a practical point of view, the primary interest is in the hovering and maneuvering of flow-aligned cylinders or other platforms of about 1 m in length and 30 cm in diameter or depth. Hovering and other maneuverings such as yawing include station-keeping in sea states and in currents. Ideally, such platforms should have high efficiency, with minimal input of momentum into the water and very little acoustic radiation. It is also desirable to have novel requirements such as a built-in disturbance rejection capability (robustness) and rational integration of controllers, actuators, and sensors. Concepts that have a rigorous mathematical formulation are preferred, and a synthesis of bio-physical advances shows that this formulation needs to be nonlinear in character to achieve self-regulation and disturbance rejection properties. (Theoretical definition of self-regulation and why this is a nonlinear process is given in [11.15]; theory showing why the motion of animals is determined by olivo-cerebellar dynamics which is a nonlinear self-regulating process is given in [11.24–29]; and the theory of why sensing, control, and actuator hydrodynamics in swimming and flying animals are likely described by similar self-regulating equations, is given in [11.28].)

Below, the flapping fin and the transitional vortices produced are treated as coupled nonlinear oscillators. The transitional (reverse Karman) vortex production process, which is the key to thrust, is shown schematically in Fig. 11.2 for a pectoral fin [11.15, 28]. A leading-edge vortex (LEV) on the fin (Fig. 11.2c) and a reverse Karman vortex train (Fig. 11.2b) in the wake are produced when the Strouhal number (St) and pitch amplitude (and Reynolds number) are appropriate (Fig. 11.2f). Due to the motion of the stagnation point [11.15], symmetry is broken [11.29]. As a result, the lift force is enhanced and thrust is produced. This vortex becomes uniform along the span when an appropriate twist is applied (Fig. 11.2d,e). Figure 11.2f shows

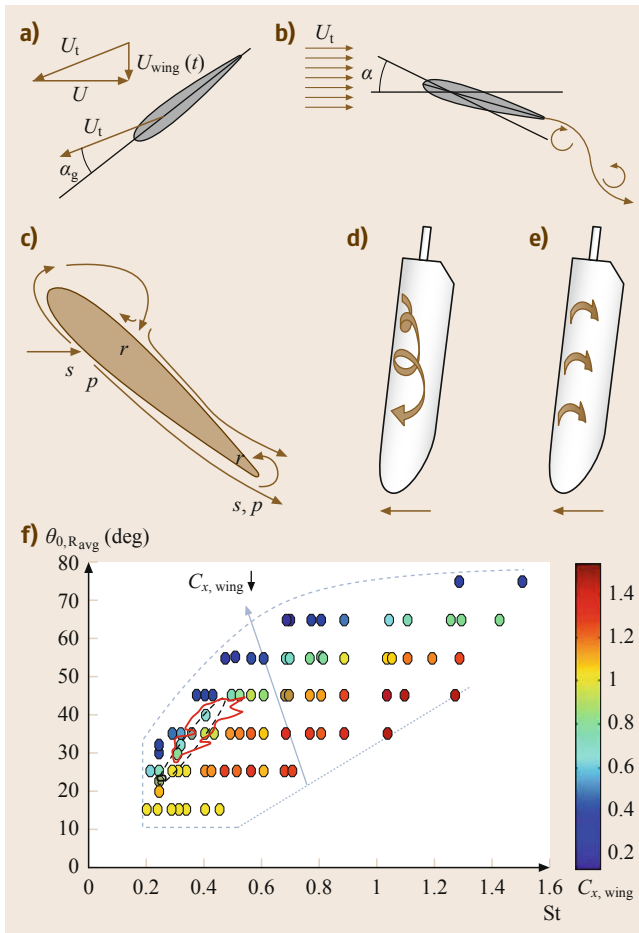


Fig. 11.2a–f Schematics of flow features in a penguin-like flapping pectoral fin: **(a, b)** fin–wake coupling; **(c)** flow bifurcations; and **(d, e)** leading-edge vortex (spirals on fins) in untwisted fins **(d)** and fins twisted spanwise **(e)**; the leading-edge vortex enhances lift force; **(a)** the geometric angle of attack of the fin α_g is determined from the forward fin velocity U and the wing velocity $U_{wing}(t)$, and U_t is total velocity; **(b)** the wake vortices, however, alter the motion of the stagnation points resulting in an effective angle of attack α ($\neq \alpha_g$), and the symmetry breaking by the motion of the stagnation point leads to thrust production; **(c)** streamline symbols are: s (stagnation point), r (reattachment), p (separation); **(d–e)** arrows: direction of fin motion. **(f)** Strouhal number (St) – pitch amplitude (θ_0) parameter space where cruising hydrodynamic efficiency in a single flapping and twisting fin is maximum (> 0.57 ; region marked by broken ellipse and red lines), or maximum forward thrust (deep red symbols) is produced; thrust is produced only in the region marked by the broken lines; the large arrow indicates direction where forward thrust ($C_{x,wing}$) drops (after [11.15, 29]) ◀

where a fin, hinged at one end, is operated for efficient cruising (area enclosed by red lines) or maximum thrust (red symbols). Efficiency and thrust reach maximum values at lower and higher values of St , respectively, while θ_0 remains in the same range; the angle of attack is lower and higher, respectively. Note that the effects of the orthogonal fin roll (given by St) and pitch oscillations (θ_0) are coupled.

11.1.1 Flapping Fin Propulsion Technology

Flapping fins can impart a great deal of momentum to the water because the frequency of flapping can be increased without being constrained by the size of any internal reservoir. Rigid or nearly rigid fins can be scaled up better compared to highly flexible fins as in sunfish. Flapping fins when hinged at one end

produce a LEV that remains pinned to the fin due to Coriolis forces [11.30]. As the measurements in [11.16, Fig. 9] show, due to delayed stall, higher lift forces are produced by flapping fins, which can operate at spatiotemporal angles of attack higher than the (first) stall angle. When the fin is flapped at the natural frequency of vortex shedding and the pitch amplitude is commensurate (between 20° and 40°) with the Strouhal number (St) in the range of 0.2–0.4, at a phase difference of about 90° between pitch and roll, efficiency reaches a maximum value (of about 0.60 in rigid fins of low aspect ratio) (Fig. 11.2f) [11.15]. Swim rules have been developed for optimal yawed swimming and yawing [11.3, 15–17, 19]; (the summary is presented later in Table 11.1). Further optimal swim rules have been developed by calibrating a cruising cylinder appended with six flapping fins in a tow tank [11.3]. The vehicle maturities considered here have been achieved by flapping the fins at these optimal conditions and by developing controllers to accomplish the flapping [11.14, 19].

In the vehicles considered here, there is no buoyancy control device because the multiple fins appended to the hull produce the required degrees of freedom with added simplicity. This is useful in rivers and estuaries where salinity can vary greatly. Forces and moments in all directions are controlled by phased oscillation of the flapping fins.

Table 11.1 Summary of flapping fin parameters for optimization of efficiency and thrust during cruising and yawing. Also included are characteristics of wall-shear stress (τ_w) patterns over the flapping fin for these flapping fin parameters: $\phi_0 = 30^\circ$, $\psi = 90^\circ$, $\theta_{t0} = 0^\circ$

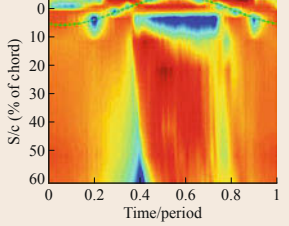
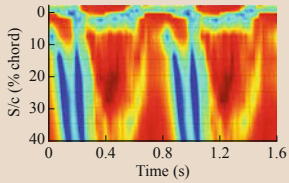
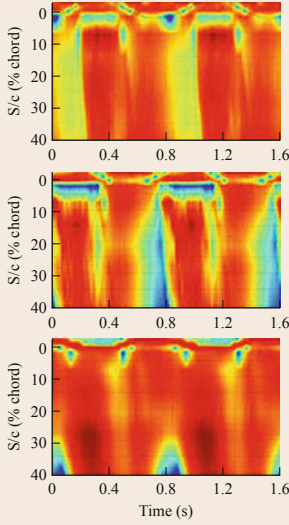
Cruising, hovering, or yawing	Fin kinematics: straight ($\theta_{Bias} = 0$), or yaw ($\theta_{Bias} \neq 0$) swim	Fin optimization parameters based on thrust or efficiency	Salient features of $\tau_w(t)$ on fin surface (blue: low, red: high wall-shear stress); both pressure and suction surfaces are shown; sinusoidal line: stagnation point trajectory; vertical axis: % chord, horizontal axis: time	
Cruising or hovering in straight path (that is, not yawing)				
Cruising: $U > 0$ $U_{wing}/U_t \rightarrow 0$ $Re_c = (30 - 130) \times 10^3$	$\theta_{Bias} = 0^\circ$ $\phi_0 = 30^\circ$ $\psi = 90^\circ$ $\theta_{t0} = 0^\circ$	$0.25 \leq St \leq 0.40$ $20^\circ \leq \theta_0 \leq 45^\circ$ $\eta > 0.57$ $C_{x,\eta} = fn(St, \theta_0)$ (higher θ_0 for higher St)	Spanwise bands of low τ_w near the leading edge, followed by high τ_w over the chord away from the leading edge when the stagnation point is advancing to the facing side of the fin during half the cycle of oscillation; during the remaining half of oscillation, as the stagnation point recedes to the other side, a thin band of high τ_w near the leading edge is followed by low τ_w over the remaining part of the chord	
Hovering: $U = 0$ $U_{wing}/U_t \rightarrow 1$	$\theta_{Bias} = 0^\circ$, $\phi_0 = 30^\circ$, $\psi = 90^\circ$, $\theta_{t0} = 0^\circ$,	$C_x = fn(f^2)$ $\theta_0 = 45^\circ$	Bands of low τ_w along oscillating stagnation line; this is followed by one pair of a band of low τ_w along the chord per cycle, followed by high τ_w over $s_c/c > 0.05$	
Yawing while cruising or hovering				
Cruising: $U > 0$ $U_{wing}/U_t \rightarrow 0$ $Re_c = (30 - 130) \times 10^3$	$ \theta_{Bias} < 20^\circ$ $\phi_0 = 30^\circ$ $\psi = 90^\circ$ $\theta_{t0} = 0^\circ$	$0.25 \leq St \leq 0.40$ $20^\circ \leq \theta_0 \leq 45^\circ$ $\eta > 0.57$ $C_{x,\eta} = fn(St, \theta_0)$ (higher θ_0 for higher St)	Oscillating leading-edge stagnation point for zero (top, 0°), positive (middle, 10°), and negative (bottom, -10°) pitch bias; bands of low τ_w for $0^\circ < \theta_{Bias} < 20^\circ$: spanwise near leading edge as for no yaw plus some chordwise patterns; for $0^\circ > \theta_{Bias} > -20^\circ$: mostly high τ_w and attached flow	

Table 11.1 (continued)

Cruising, hovering, or yawing	Fin kinematics: straight ($\theta_{Bias} = 0$), or yaw ($\theta_{Bias} \neq 0$) swim	Fin optimization parameters based on thrust or efficiency	Salient features of $\tau_w(t)$ on fin surface (blue: low; high wall-shear stress); both pressure and suction surfaces are shown; sinusoidal line: stagnation point trajectory; vertical axis: % chord, horizontal axis: time	
Yawing while cruising or hovering				
Hovering: $U = 0$ $U_{wing}/U_t \rightarrow 1$	$0^\circ < \theta_{Bias} < 45^\circ$ $\phi_0 = 30^\circ$ $\psi = 90^\circ$ $\theta_{t0} = 0^\circ$	$C_x = f(\theta)$ $\theta_0 = 45^\circ$	With increasing positive pitch bias angles, regions of low τ_w increase; one pair of brief bursts of low τ_w extend over chord per cycle of fin oscillation; oscillating stagnation line is a band of low τ_w as when $U = 0$ and $\theta_{Bias} = 0^\circ$	
Hovering: $U = 0$ $U_{wing}/U_t \rightarrow 1$	$0^\circ < \theta_{Bias} < -45^\circ$ $\phi_0 = 30^\circ$ $\psi = 90^\circ$ $\theta_{t0} = 0^\circ$	$C_x = f(\theta)$ $\theta_0 = 45^\circ$	With decreasing pitch bias angles below 0° , the chordwise bands of low τ_w partly become compact and shift mostly down chord	

Note: When τ_w is very low, the local fin boundary layer approaches separation. When τ_w is very high, the boundary layer is attached and may be accelerating. The topology of the near-wall flow over the fin can be defined by critical points such as saddles and foci; in the flapping fins, these flow bifurcation points can be identified: spatiotemporal stagnation point, separation and reattachment points [11.15]

11.2 Theoretical Foundation of Animal-Inspired Hydrodynamics and Control

Flapping fins are nonlinear oscillators. In the case of a drag-producing cylinder in a stream, the lowest order solution of the Navier–Stokes equation of the wake instability reduces to a van der Pol equation [11.31, Appendix]. The latter equation applies also when the cylinder is freely suspended and is galloping (at the natural frequency) [11.32]. Obviously, the cylinder can be replaced by a low-drag foil and the van der Pol form of the Navier–Stokes equation would still describe the lowest order solution of the wake instability. It has been shown [11.15] that the van der Pol solution can be extended to a flapping fin (i.e., if the fin wake is perturbed by a flapping fin motion) oscillating at the natural frequency when the drag wake is replaced by a thrust wake after symmetry breaking [11.29]. In other words, in the transitional range of Reynolds number, vortex-propelled animals can be described by nonlinear oscillators as indeed was implied earlier by *Karman* and *Burgers* [11.1] and *Lighthill* [11.2] and *Bandyopadhyay* et al. [11.15].

11.2.1 Hydrodynamics

As depicted in Fig. 11.2a,b, in the swimming animal, the oscillating surface and the vortex street couple [11.28]. The wake circulation alters the geometric fin angle of attack given by the forward velocity and the fin oscillation velocity. This mechanism allows a freely suspended flexible fin oscillating at the natural frequency and its wake vortex train to adjust to each other (lock-in) in terms of phase and energy, iterating to a low-energy system (minimal losses).

For a single fin hinged at one end that is also twisting and flapping in the optimal manner (Fig. 11.2d,e) near the natural shedding frequency of the wake instability of the nonflapping fin, the instantaneous fluctuating force F'_x produced agrees well – to a leading order particularly at high Reynolds numbers (fin chord and cruise speed-based $Re_c \approx 70\,000$) – with the van der Pol formulation given below,

$$\ddot{F}'_x - \omega_s G(F'^2_{x0} - 4F'^2_x) \dot{F}'_x + \omega_s^2 F'_x = \omega_s TR_{avg} \dot{\xi}, \quad (11.1)$$

where

$$\begin{aligned}\xi(t) &= \phi(t) + \theta(t), \\ \phi &= \phi_0 \sin(2\pi ft), \\ \theta(t) &= \theta_0 \sin(\omega t + \psi) + \theta_{\text{Bias}}, \\ \omega_s &= 2\omega\pi \frac{StU}{A}, \\ A &= 2\phi_0 R_{\text{avg}}.\end{aligned}$$

F'_x is the fluctuation in force, and F'_{x_0} is the amplitude of F'_x ; $G(=0.02)$ and $T(=0.5)$ are constants (determined by trial) that affect the shape and the blur of the oscillatory solution (the limit cycle), respectively. In other words, the flapping (rolling and pitching) fin is a nonlinear oscillator and has a limit cycle oscillation (LCO) [11.15]. (The roll, pitch, and twist oscillation of the hinged fin may be seen to act as the $I_{\text{exti}}(t)$ term (see olivo-cerebellar control Sect. 11.2.2 below) to the nonlinear oscillator arising out of the natural vortex shedding of the nonflapping fin.)

Flapping Fin Parameters for Cruising and Maneuvering

Table 11.1 summarizes the fin kinematics that a controller (in the BAUV, SPLINE, and Razor vehicles, Sect. 11.3) uses for optimization of thrust and efficiency during cruising, hovering, and yawing. The total forward velocity is much higher than the wing velocity (which is cross-stream) during cruising, and these velocities are nearly equal during hovering (the forward speed is zero during hovering). Biasing the fin pitch at half the required yawing angle is the key fin setting required for yawing. For optimization of efficiency, the controller makes use of the observed direct coupling between Strouhal number St , whose definition includes roll oscillation amplitude ϕ_0 and pitch amplitude θ_0 ; a higher pitch amplitude of about 40° is used when St is near 0.40, and a lower pitch amplitude of 20° is used when St is near 0.25 (Fig. 11.2f) [11.15]. Also, note that in a single flapping fin, thrust is a function of the square of the flapping fin frequency f for given pitch amplitude and forward speed [11.15, 19].

The flapping fin mechanism can be understood by observing that the forces produced are describable by van der Pol (11.3) [11.15] or Stuart Landau nonlinear oscillators [11.28]. Using the equation for the latter oscillator, it has been shown theoretically that a coupling exists between the fin and the wake [11.28]. Table 11.1 can be viewed as tuning of the oscillator under various performance requirements. The rightmost column in Table 11.1 summarizes the wall shear stress on the fin for the fin kinematics given in the other columns. Characteristic patterns can be observed:

1. The point of stagnation oscillates, shifting from one pressure side of the fin to another pressure side as the pressure and suction roles of the fin surfaces alternate.
2. Downstream of the stagnation line and on the suction side, a generally spanwise low-wall-shear region develops, indicating the presence of a LEV.
3. Chordwise low-wall-shear bands appear in the suction side in hovering and yawing fins, indicating a complex and less efficient surface flow.

11.2.2 Animal-Like Motion Control Laws and the Principles of Integrated Design

We describe the unmanned underwater vehicle (UUV) design to be integrated when the actuators (fins), controllers, and sensors have similar laws of dynamics. In the case of animal-inspired swimming, these will be equations of nonlinear oscillators.

We assume that the principles of integrated design are derived from the olivo-cerebellar motion control laws [11.24–27, 33], as evidenced by the dynamics of the inferior-olive (IO) neurons that are responsible for motion and balance in all mammals, from rats to human beings [11.24, 25]. We first consider the motion control laws and then how the controller, actuator, and sensors are integrated in a common framework of dynamic systems mathematics.

The motion control laws are self-regulating. In such control, a sensor is not needed for error estimation with respect to a reference because a conventional closed control loop is not present. In other words, these controllers reject disturbances, which make them robust. (See [11.3, 28] for discussion of self-regulation.) Owing to this robustness, the controllers have remained unchanged in many animals.

The olivo-cerebellar dynamics of an IO neuron ($i = 1, 2, \dots$) can be represented by two coupled nonlinear oscillators (u_i, v_i) and (z_i, w_i) as given below [11.26, 27],

$$\begin{bmatrix} \dot{u}_i \\ \dot{v}_i \\ \dot{z}_i \\ \dot{w}_i \end{bmatrix} = \begin{bmatrix} k(\varepsilon_{\text{Na}})^{-1}(p_{\text{iu}}(u_i) - v_i) \\ k(u_i - z_i + I_{\text{Ca}} - I_{\text{Na}}) \\ p_{\text{iz}}(z_i) - w_i \\ \varepsilon_{\text{Ca}}(z_i - I_{\text{Ca}}) \end{bmatrix} + \begin{bmatrix} 0 \\ 0 \\ 0 \\ -\varepsilon_{\text{Ca}} \end{bmatrix} I_{\text{exti}}(t), \quad (11.2)$$

where the variables (z_i, w_i) are associated with the subthreshold oscillations and low-threshold (Ca-dependent) spiking, and (u_i, v_i) describe the higher threshold (Na^+ -dependent) spiking (this is similar to FitzHugh–Nagumo equation). The constant parameters ε_{Ca} and

ε_{Na} control the oscillation time scale; I_{Ca} and I_{Na} drive the depolarization levels; and k sets a relative time scale between the uv - and zw -subsystems. The nonlinear functions are

$$\begin{aligned} p_{iu}(u_i) &= u_i(u_i - a)(1 - u_i), \\ p_{iz}(u_i) &= z_i(z_i - a)(1 - z_i). \end{aligned}$$

The function $I_{\text{exti}}(t)$ is the extracellular stimulus, which can be used for the purpose of control, such as phase synchronization. Note that in a UUV, we do not need to be concerned with the ionic interpretations of the variables and constants; we are only concerned with the generic nonlinear dynamics [11.28].

The (u_i, v_i) oscillator can generate spikes (analogous to neural action potential), but this feature has not been used in the context of UUV maneuvering. The (z_i, w_i) oscillator, however, has been used successfully to synchronize the phase of a six-finned vehicle [11.33].

The salient features of this approach to control compared with conventional engineering controllers (i.e., proportional, integral, derivative (PID) controllers) are that no sensors are required, no reference is required, the controller has built-in disturbance rejection ability, and, in principle, the controller has no size or time scale limitation.

The lower oscillator in (11.2) can then be written as

$$\ddot{z}_i + F(z_i)\dot{z}_i + kz_i + \varepsilon I = 0, \quad (11.3)$$

where F is a cubic polynomial function and k is a constant if $I_{\text{exti}}(t) = 0$. Equation (11.3) resembles Lienard's oscillator (in contrast, the function F is a well-defined quadratic in the more familiar van der Pol oscillator [11.34, p. 13]). The oscillator exhibits a closed orbit Γ_i in the state space $(z_i - \dot{z}_i)$, that is, $(z_i - w_i)$, which is also known as LCO, with the constant parameters determining the form of Γ_i .

Below, we consider the notions of integrated design and nonlinear sensing because they are theoretically attractive.

Principles of Integrated Design

Swimming animals offer clue to homing, autonomy, and station keeping. The mechanisms are at a theoretical stage of understanding and we touch upon them notionally to spur future work. The principles of integration of the controller, actuator, and sensor are based on the hypothesis of *persistent synchrony with the environment* which after all should enhance mission effectiveness (pursuit of food, mating, and evasion in the case of animals). According to this hypothesis, not only the controller, but also the actuator and the sensor must follow similar dynamics as given essentially in (11.1)–(11.3). We have shown that the actuator does indeed follow laws similar to olivo-cerebellar dynamics [11.15]. It has been shown that it is beneficial for a UUV if olivo-cerebellar dynamics is a common principle of the three elements of the platform. In [11.28], it is shown that an integrated design accelerates homing if we build-in 10–15% of handedness.

Nonlinear Sensing as a Theoretical Requirement of Autonomy

Nonlinear acoustic sensing is another piece of the autonomy puzzle which however is the least developed of the three components, namely sensor, actuator, and controller. Most hydrophones are based on linear vibration of transducers which require lines of them for improved aperture. In [11.35], an alternative theoretical foundation is given based on nonlinear LCO of tiny three-dimensional transducer elements. (These are similar to cilium sensors – widely used by animals.) This transducer has a built-in disturbance rejection (of vibration, e.g.) property. Furthermore, by the use of the property of metachronism in a cluster of such nonlinearly oscillating transducers, acoustic sensing methodologies can be miniaturized and aperture can be increased.

The above rationale for the integration of actuators, controllers, and sensors, together with the need to develop nonlinear oscillatory versions of these three individual systems, gives a mathematically founded basis of autonomy.

11.3 Description of Biology-Inspired Vehicles of Emergent Maturity

Tables 11.2 and 11.3 summarize the salient features of the more mature bio-inspired and bio-mimicry vehicles, respectively. Brief descriptions of the bio-inspired vehicles and sample results are presented in Figs. 11.3 through 11.6. Table 11.4 summarizes the salient features of the engineering controllers (i. e., PID gain, adaptive, or cascading controllers) and olivo-cerebellar controllers that were crucial to demonstration of the low-speed maneuverability of the bio-inspired vehicles.

Figure 11.3a shows the first generation of the six-finned cylindrical BAUV; Fig. 11.3b shows the BAUV mated with a dolphin-inspired interaural time-differencing bio-sonar; and Fig. 11.3c presents representative results showing the tracks of the vehicle maneuvering around obstacles while pointing the bio-sonar at the target; these experiments were carried out in an acoustic test facility.

Figure 11.4a is a schematic of a cable with sensors (such as hydrophones and accelerometers) held taut between two flapping fin propulsion units. Figure 11.4b is a photograph of the components inside the self-propelled line array (SPLINE) hull. Figure 11.4c shows the cable being turned around a pole by one propulsion unit, while Fig. 11.4d gives representative measurements of turn radius, which can be held constant as desired.

In the meta analysis in Fig. 11.1, the trend line of the cruise data of the very large engineering vehicles and the red muscle data of the animals like sharks converge for displacement volumes from 0.01 to 1.0 m³, although the force production mechanisms are different – steady-state lift properties of fixed blades in the former and pinned-LEV type modified dynamic stall of flapping fins in the latter. Based on this cue, a propulsor was

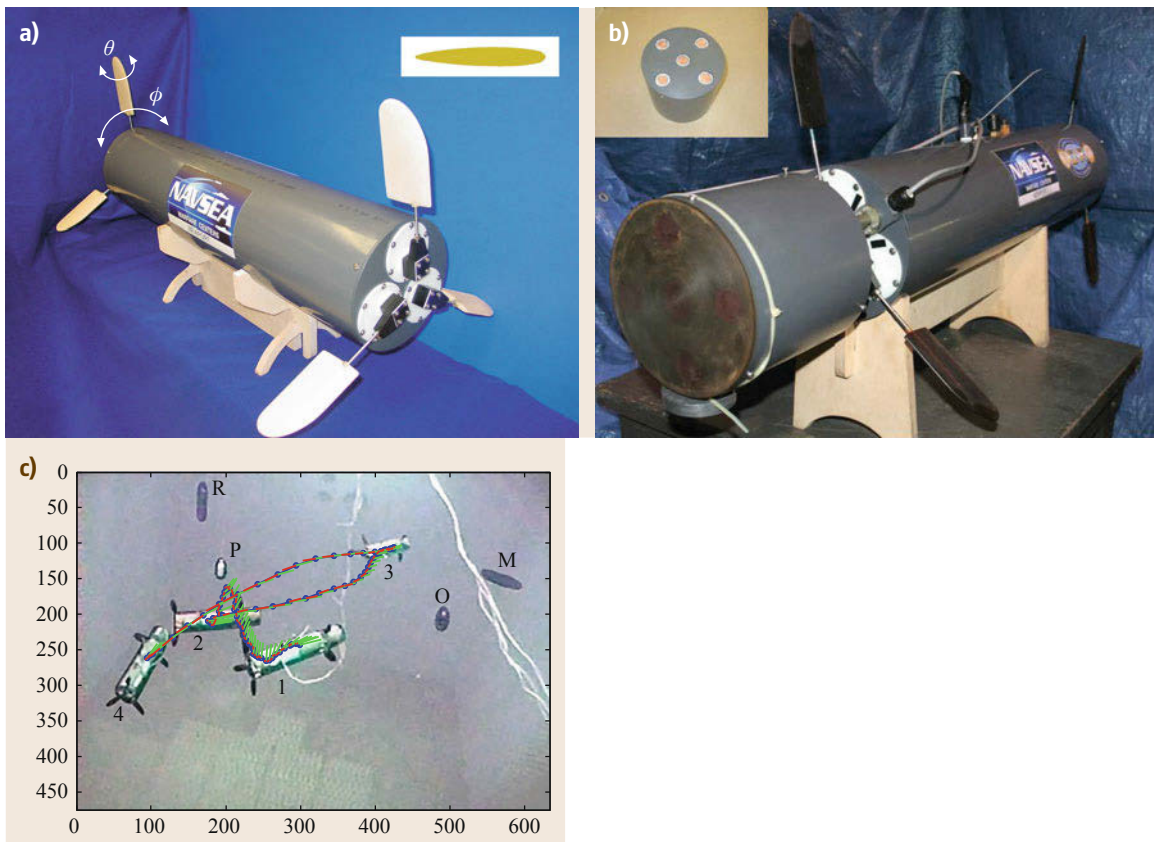


Fig. 11.3 (a) Photograph of BAUV, the first generation of the NUWC six-finned bio-inspired UUV. The inset shows the fin section (after [11.19]); fin pitch (θ) and roll (ϕ) oscillations are shown. (b) BAUV mated with approximated *bio-sonar* in front; inset shows the four (interaural) receivers and the central transmitter of the bio-sonar (after [11.36]). (c) Bio-sonar mounted BAUV navigating (1–4: increasing time) obstacles (M, O, P, R) in the NUWC Acoustic Test Facility (after [11.36]); water tank size: 10.6 m (depth) \times 12.2 m \times 18.3 m; axes: in pixels

Table 11.2 Summary of more mature bio-inspired underwater platforms

Platform name, institution, figure, and reference	Mission, purpose, comments	Typical dimensions	System and instrumentation	Biology principle, and modes of operation	Comparative performance statement with respect to conventional technology	Future work
BAUV, NUWC, Fig. 11.3 [11.19]	Exploratory development of flapping fin propulsion and olivo-cerebellar control technology	Cylindrical hull length 0.91 m, diameter 0.22 m; fin chord 7.5 cm, span 15 cm	Dolphin-inspired interaural time-differencing bio-sonar; depth sensor; onboard power source and data storage	Flapping fins: low-aspect ratio fins hinged at one end, pitches at 1/3rd chord from leading edge; LEV high lift (pinned-LEV type modified dynamic stall). Control: (a) olivo-cerebellar dynamics control – self-regulating dynamics (LCO); or (b) PID control using synthesis of cycle-averaged fin forces	Exquisite hovering and low-speed maneuverability; low cruise drag at low forward speeds; propulsion power/displacement is shark-like; more efficient than cross-tunnel thruster-based design	Mission-driven self-exploration of optimal maneuvering with olivo-cerebellar dynamics
SPLINE, NUWC, Fig. 11.4 [11.14]	Exploratory development of self-propelled line array concept of persistent surveillance	Cylindrical hull length 1.57 m, diameter 0.2 m; fin chord 9 cm, span 21 cm; cable length between propulsion units 7.3 m	Depth sensor, compass, inertial navigation unit, tilt sensor, line array tension load cell; onboard power source and data storage	Flapping fins: LEV high lift (pinned-LEV type modified dynamic stall); control: PID gain, adaptive, or cascading control using synthesis of cycle-averaged fin forces	Hovering and low-speed maneuverability; low cruise drag at low speeds; propulsion power/displacement is shark-like [11.3], Fig. 11.1; more efficient than cross-tunnel thruster-based design	Station-keeping in highly disturbed environment (high sea states)

Table 11.2 (continued)

Platform name, institution, figure, and reference	Mission, purpose, comments	Typical dimensions	System and instrumentation	Biology principle, and modes of operation	Comparative performance statement with respect to conventional technology	Future work
RAZOR, NUWC, Fig. 11.6 [11.8, 37, 38]	Multimission expeditionary autonomous UUV; harbor defense including swimmer interdiction, bottom surveys, hull inspection, and search, classify, and map missions with 360° sensor coverage of target; payload > 0.0566 m ³ ; 100 m depth rating	Delta hull; modular design; overall length 1.7 m × depth 0.27 m × 0.76 m wide plus fin span; rear thruster; four rigid fins; two-man portable	Streaming of actuated imaging sonar and video camera; interdiction devices; radio frequency (RF) antenna, camera and global positioning system (GPS) on mast; depth sensor, doppler velocity log (DVL), inertial measurement unit (IMU), onboard power source, and data storage; onboard and tethered programming; field replaceable energy, endurance 6–20 hr with one-three batteries (1.5 kW/hr/tolerant lithium battery); WiFi 54 Mbs secure	Flapping fins: LEV high lift (pinned-LEV type modified dynamic stall); control: (a) hovering and low speed; PID control using synthesis of cycle-averaged fin forces; (b) higher speed: rotational speed control of conventional rotating propulsor; hull planform and fin layout bear similarity to turtles [11.39] but for the rear propulsor, the antenna, and the launch tubes	Exquisite hovering and low-speed maneuverability; more efficient than cross-tunnel thruster-based design; energy efficiency over conventional means of propulsion	Development of controller that transitions from flapping fins to rotating propulsion
SLOSER, NUWC, Fig. 11.5 [11.40]	Platform mobility	Without shroud: NACA 0012-34 section fin chord 7.5 cm, 16 cm span, abstracted penguin wing planform; with shroud: 0.29 m internal diameter 7.5 cm chord shroud with 7.5 cm chord 8.9 cm span similar fin section	Power diagnostics for efficiency tracking	Fins can flap (roll and pitch) or spin as commanded; flapping fins: LEV high lift (pinned-LEV type modified dynamic stall); spinning fins: steady-state fin lift properties	Sloshing mode at hovering and low forward speeds complements high forward speeds with spinning mode	Simultaneous rolling, pitching, and twisting fins; vectored thrusting; integration with olivo-cerebellar dynamics controller

Table 11.3 Summary of more mature underwater platforms based on bio-mimicry

Platform name, institution, and reference	Mission, comments	Typical dimensions	System and instrumentation	Biology principle	Comparative performance statement with respect to conventional technology	Future work
Robotuna MIT [11.22, 23]	Purpose: Study of fish swimming in controlled manner; appears to support Gray's paradox that the drag of the swimming Robotuna (with oscillating tail) is less than that of the straight (that is, non-flapping, rigid) Robotuna	Seeks to mimic full scale fish: 70 km/hr; skipjack tuna (0.91 m × 35 lbs) – Blue fin tuna (4.27 m × 680 kg); Robotuna: six brushless DC servomotors, pulleys, and cable tendons drive eight discrete rigid vertebra; skin: thin layer of flexible reticulated foam covered by a conformal Lycra sock	Not available	Flapping caudal fin propulsion; flexible body shaped as Giant Dania; a wave of variable amplitude passes from nose to tail for propulsion	Directly demonstrated fish thrust production mechanism; tuna form has scalability	Burst of acceleration; fast start; understanding of hydrodynamic mechanism, reduction of power consumption due to the robotic drive; Robopike and GhostSwimmer are derivatives
Finnegan MIT [11.39]	Purpose: explore fin-based swimming in turtle-shaped vehicle configuration; 10 m depth operation	2 m × 0.6 m × 0.5 m; foils protrude 0.4 m from each side, 0.1 m average chord	Onboard power source and data storage; preprogrammed mission; inertial navigation; modified Rodrigues parameter linear control algorithm; open loop control; navigation sensor; pressure sensor; Doppler velocity logger	Mimics turtle; four flapping rigid fins for propulsion appended to a rigid turtle-like hull; linearized engineering control	Improvement in maneuverability by reduction in stability; banked and twisting turns (assisted by hull shape); exceeds turning performance of AUV by a factor of two; minimum turn radius = 0.7 times body length	Not available
GhostSwimmer Boston Engineering Corp. [11.21]	Reconnaissance; hull inspection; oceanographic mission	See Robotuna above	Compact electronics compared to that in Robotuna	Dorsal, pectoral, and caudal fins; flexible body shaped as blue fin tuna;	Small radius turning ability	Efficient actuation of flexible surface, speed enhancement

Table 11.4 Summary of features of controllers of bio-inspired underwater platforms

Platform name, institution, figure, and reference	Control problem scope	Control principle/laws	Summary of demonstration	Comparative statement with respect to conventional approach without bio-inspiration or biomimicry	Future work
BAUV, NUWC, Fig. 11.3 [11.19]	Exploration of maneuvering and hovering in a rigid cylindrical hull appended with six flapping fins (with internal actuator constraints)	Open loop control; cycle-averaged forces and moments are given by fin kinematic parameters based on experimental calibration; fin forces act at one point of fin at a distance of average radius (R_{avg}) from roll axis; net force and moment from synthesis of individual fin forces and moments, and fin placement on hull; PID	Coordination of multiple fins to achieve high maneuverabilities (listed in Sect. 11.5). Solution accommodates inherent constraints of actuator placement within hull.	Far more maneuverable and energy efficient by a factor of 2 compared to cross-tunnel thruster-based vehicle design; no separate buoyancy control is needed	Integration of olivo-cerebellar dynamics with nonlinear sensing and flapping fin propulsion
SPLINE, NUWC, Fig. 11.4 [11.14]	Tension and position control of a short-length cable in laboratory and tidal basin using flapping fin propulsors at each end	Open and closed loop control; approach similar to that in BAUV; PID	Turning of a short-length cable around a pole at a given depth while holding it taut with propulsion at one end; holding of commanded tension and position (horizontal or vertical) in cable with propulsion at one end; swimming of the short-length cable to commanded depth while holding it taut using propulsion at both ends	Minimal input of momentum into water; smoother transition between maneuverings; no separate buoyancy control is needed	Station-keeping in sea state while holding the cable taut
RAZOR, NUWC, Fig. 11.6 [11.8, 37, 38]	Synthesis of four flapping fins and a thruster	Open and closed loop control; approach similar to that in BAUV; control of a thruster for cruising; PID	Coordination of fin propulsion and thrusters; see list of surface and underwater maneuverings in Sect. 11.5.	Fin propulsion for hovering and low-speed maneuvering; thruster does higher speed cruising; no separate buoyancy control is needed	Controller for smooth transition from flapping fin propulsion to thrusters
BAUV, NUWC, Fig. 11.3 [11.33]	Transition of animal-like control to UUV	Limit cycle – olivo-cerebellar dynamics; phase synchronization using SPR property of inferior-olive neurons (SPR-self-referential phase reset [11.26])	Demonstrated faster swimming when phase difference between multiple fins is appropriate	Olivo-cerebellar dynamics has disturbance rejection property; also has phase synchronization property when external impulse is applied; no separate buoyancy control is needed	Station-keeping, gait change, integration with sensors and artificial muscles

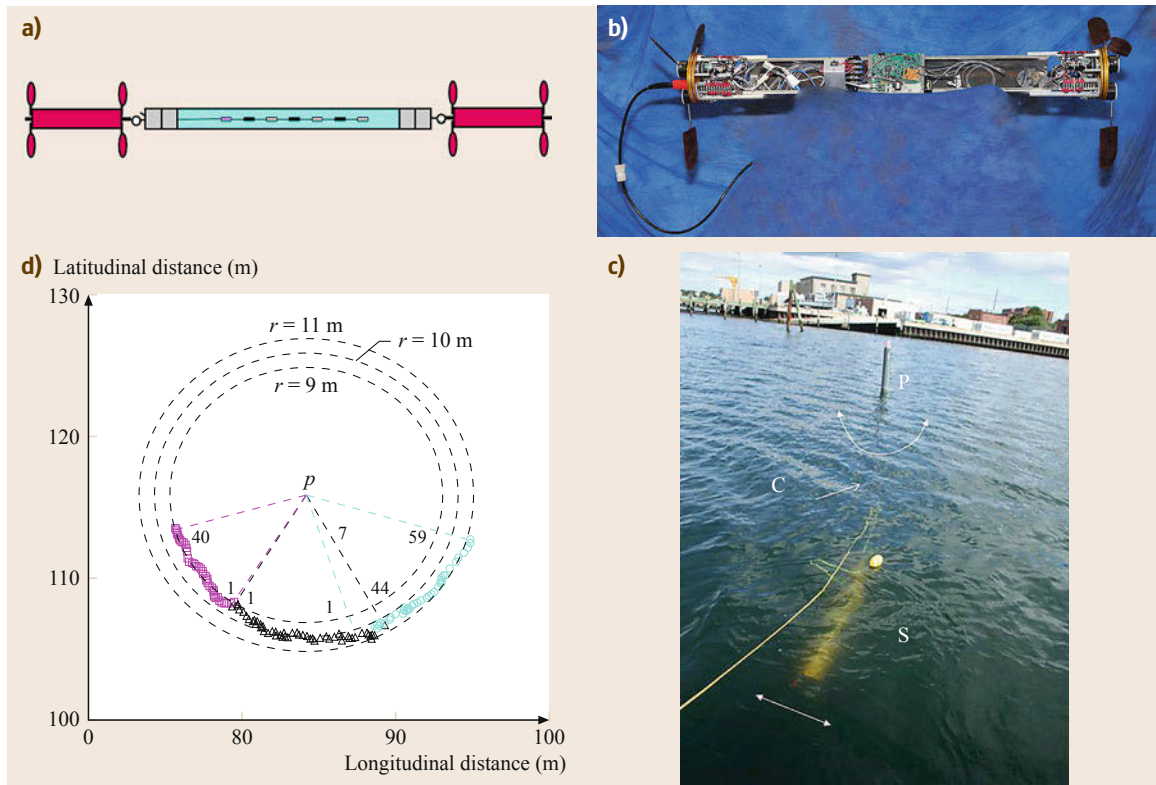


Fig. 11.4 (a) Schematic of line array held taut by a pair of SPLINE propulsors. (b) Photograph of the instrumented inside of the cylindrical hull of the SPLINE propulsor. (c) A SPLINE propulsor turning a short-length cable about a pole (after [11.14]). (d) Measurements of turn radius; P is the pole in (c), 7 denotes the position of the 7-th hydrophone, the numerals indicate the direction of increase in time, r is radius, three different runs are shown. In (c): P – pole, C – cable, S – SPLINE; \leftrightarrow indicate directions of turning

conceived where the blades could both flap and spin as needed. Figure 11.5a is a photograph of such a novel propulsor where the blades can spin as in conventional propulsors while holding the pitch angle fixed, or the blades can slesh (roll and pitch represented by ϕ and θ , respectively). Figure 11.5b shows the internal blade motor drives and controller housed in the hub. This version of the propulsor also shows a shroud normally used for reduction of acoustic radiation. In the configuration shown in Fig. 11.5a, the shroud is not present and the blades have a boundary layer fence on both sides near the tip. Figure 11.5c shows that thrust can indeed be produced in the spinning and sloshing modes – lower levels of thrust in the sloshing mode and higher levels in the spinning mode.

Figure 11.6a is an outer view of the RAZOR vehicle, and Fig. 11.6b is the RAZOR vehicle mated with the dolphin-interaural spacing bio-inspired sonar shown in Fig. 11.3b. This vehicle has undergone an exten-

sive outdoor capability demonstration (Table 11.2 and Sect. 11.5).

Of the seven biorobotic platforms and devices in Tables 11.2 and 11.3, three disparate platforms – namely, the SPLINE, RAZOR, and GhostSwimmer – are more focused on missions. Judging from this small but varied sample, tentatively speaking, *uncommon low-speed mission in disturbed environments may be the forte of biorobotics* (these vehicles remain to be tested in challenging currents and sea states; Sect. 11.5 lists maneuverings that can be termed uncommon because regular UUVs propelled by rotating propulsors alone cannot undertake those motions efficiently and with minimal disturbance input to the water). Review of the controllers in Table 11.4 indicates that the self-referential phase reset (SPR) mechanism of olivo-cerebellar dynamics may have yet unexplored far-reaching potential in precision station-keeping and platform stabilization; this might facilitate the mat-

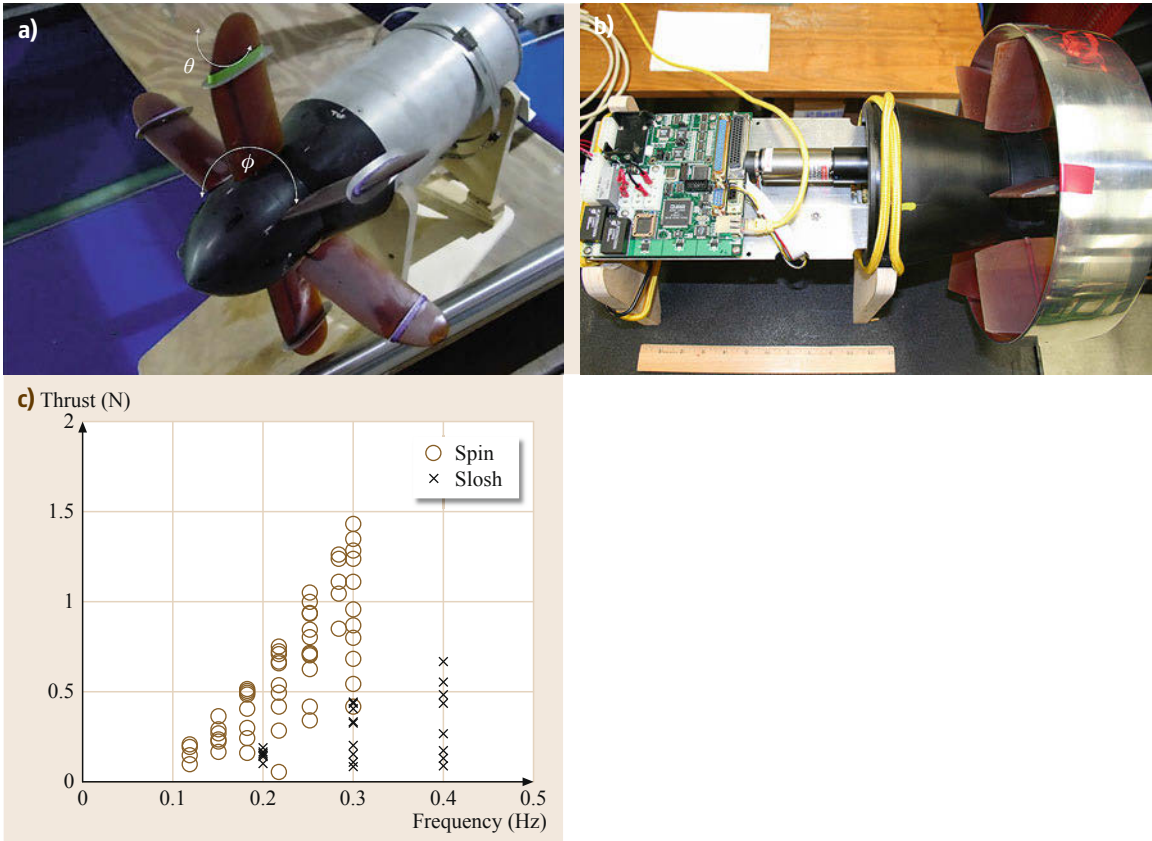


Fig. 11.5a-c Photographs of the slusher propulsor (a) and internal motor and controller (b). Note the boundary layer fence in each blade in (a). The shroud in (b) was not used in the experiments. (c) Thrust measurements when the fins are spinning, or sloshing (after [11.40]). The blade roll (ϕ) and pitch (θ) oscillations in the sloshing mode are shown in (a)

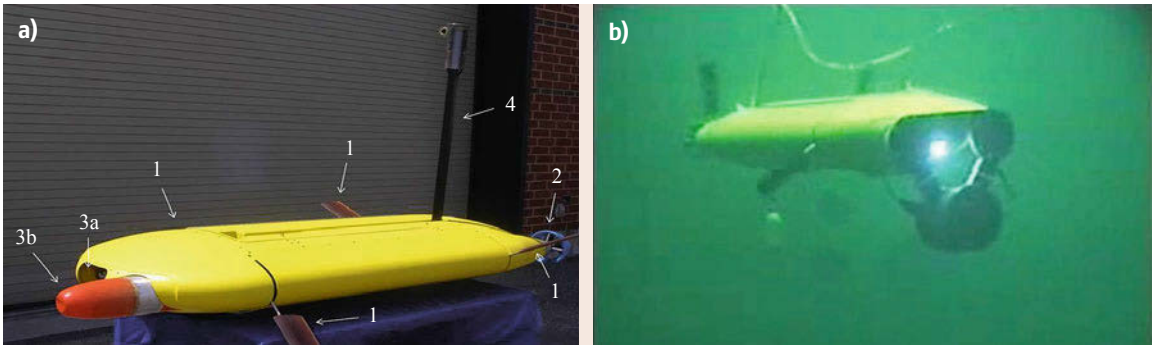


Fig. 11.6 (a) Photograph of the two-man-portable RAZOR. 1 – flapping fins, 2 – conventional rotating propulsor, 3a – launch tube, 3b – payload, and 4 – 0.76 m-long antenna. (b) RAZOR swimming with the approximated bio-sonar and front illumination (after [11.8, 37, 38])

ing of the platform with three-dimensional close-range sectional diagnostics of the target. Overall, the trend is what it should be for UUVs – that is, to provide a low-noise stable platform, in a disturbed environ-

ment, that can bring sensors in proximity to the target and make precise observations to assist bigger decision making – and, of course, do so in an autonomous manner.

11.4 Reliability, Low Power Consumption, and Disturbance Rejection of Bio-Inspired Propulsion

The six-finned SPLINE propulsor was operated in a water-filled tank held in position while pulling a fishing line. The line tension and energy consumption were recorded and are shown in Fig. 11.7. Nearly 450 h of continuous run is shown. The hull is capable of carrying the required batteries. The SPLINE propulsor has the ability to loiter at low speeds for several weeks.

The BAUV is a 40 W propulsor and the SPLINE is a 23 W propulsor. The extraordinarily low power consumption was further demonstrated by the trickle charge harvesting experiments described in [11.41, 42]. An electronic circuit was built to harvest very low lev-

els of power available from benthic microbes in littoral basins. Power is stored in 58–450 F capacitors. Operation was automated, and once the capacitors were fully charged, the SPLINE propulsor fins were activated. The 58 F capacitor was able to operate the propulsor for 165 s in a tidal basin. While this is not a long duration, the amenability of bio-inspired propulsion to renewable energy sources opens up unconventional concepts of persistent autonomous operation in the littoral basin for discussion.

An experiment was carried out by driving the flapping fin roll and pitch oscillations using a van der Pol oscillator [11.33]. The fin was oscillated near the natural frequency of oscillation for maximum efficiency. The fin roll and pitch oscillation states exhibited a LCO. An artificial electrical disturbance (a square wave) was abruptly applied to the fin to dislodge it from the set LCO; this produced large levels of transient forces, causing the fin to visibly go off track momentarily (see video in [11.33]). Although no sensor was used and no error from the reference was estimated, the thrust force and fin motions autonomously returned to the states of the limit cycle after the disturbance was removed. This experiment demonstrated that a platform in which the actuator, controller, and sensors are integrated by the self-regulation principle (as discussed in Sect. 11.2) will be autonomously robust. *We therefore posit that autonomy in animals is a consequence of the self-regulation property of nonlinear oscillators and biorobotic platforms also need to have self-regulation property.*

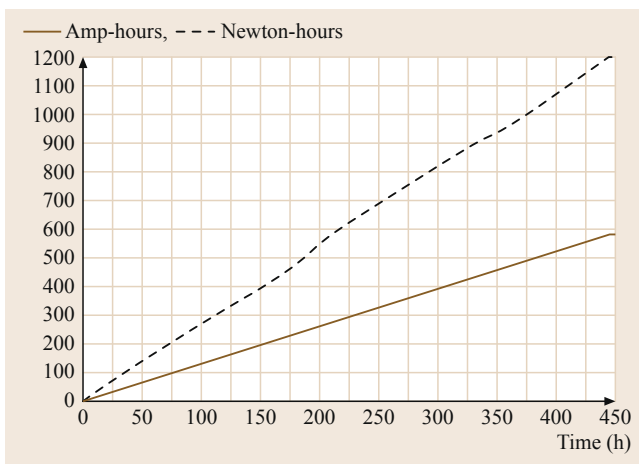


Fig. 11.7 Total energy consumption and cumulative force produced in the SPLINE propulsor, indicating long duration reliability

11.5 Demonstrated Maneuverings of NUWC Bio-Inspired Vehicles

The NUWC bio-inspired vehicles have demonstrated a variety of precision maneuverings, as listed below. Video recordings of these maneuvering motions have been made and their precision has been determined. (Listed movement precision is in cm.) The unpublished video recordings of the maneuverings are available from the author.

11.5.1 BAUV

1. Near zero meter radius clockwise and counterclockwise horizontal plane turning [11.19]
2. Parallel parking in a narrow rectangular side chamber offset from a straight tank
3. Continuous pitch up and down motion keeping vehicle center at the same location [11.19]
4. Cruising broadside in a narrow tank with minor clearance between BAUV ends and tank walls
5. Cruising while remaining yawed
6. Cruising on water surface remaining partially submerged
7. Cruising, braking, and then making soft landing on tank floor
8. Making soft takeoff from tank floor and resumption of cruising
9. Braking after cruising
10. Swimming to commanded depth and holding that depth
11. Attaching and detaching of suction cups on walls [11.43]
12. Swimming among obstacles while pointing sensors at targets [11.36].

11.5.2 SPLINE

1. Tension and position control of a fishing line or cable [11.14]
2. Simultaneous tension and position control in a fishing line or cable [11.14]
3. Swimming of a 7.3 m-long cable to commanded depth, using two SPLINE propulsors, one at each end of the cable
4. Turning of a short-length cable while holding it taut and maintaining depth in a shallow water tidal basin [11.14].

Demonstrations (1–3) were carried out in large laboratory tanks; number of propulsors: one in one end only in (1–2, 4), and one at each end in (3).

11.5.3 RAZOR

1. Cruising and remotely operated vehicle (ROV)-like maneuvering, including hovering and station-keeping
2. Numerous demonstrations of underwater and surface maneuverings carried out in Narragansett Bay, RI, in more realistic mission environments than is possible in the laboratory.

11.6 Discussion

Exploratory transitioning to utility is a filtering process applied to basic research. The material in this chapter and the papers on the underlying science [11.9, 11, 12, 15] indicate the steepness of the transition pyramid, most being eliminated quickly. Anecdotally, the transition process of underwater vehicles appears to have attained greater maturity than that of flying vehicles, if non-biology-based micro air vehicles are excluded.

The section on integrated design principles shows how disturbance-rejecting nonlinear sensing, which is currently a large gap, should be built. In view of the infancy of nonlinear sensing, we are far off from the full potential of what biology-inspired integrated platforms can offer.

In our experience, the research that transitions to utility is that where understanding is developed to the extent that a mathematical formulation of the mechanism is possible. In our design and control, scaling laws and an understanding of the cycle-averaging process have been found to be useful. To develop reliable control laws, we have experimentally calibrated full-scale actuators in the operational range whenever possible. We have not used any computational fluid dynamics because, in practice, it is postdictive and not predictive.

The value of actuator materials such as strong artificial muscles has been emphasized in the past for actuation of shape deformation of animal-like propulsors [11.7, 44–48]. However, ionic polymer, or the much heralded carbon nanotechnology is yet to make an impact on platforms of 1 m scale.

The Naval utility of platform-length scales much smaller than 1 m has not been demonstrated. This may be due to boundary between the strengths of feasible

actuation that is stiff versus highly flexible. System considerations indicate that some approaches such as jets (of squid) are inherently inefficient compared to flapping fins (of fish which impart more momentum to the water without the constraint of internal bladder size) and cannot be scaled up (the oxygen consumption rate of squid is five to seven times higher than that of fish) [11.49]. Furthermore, it does not seem to be useful to develop approaches that are vulnerable to saltwater corrosion and blockage due to biological growth, which always accompanies prolonged exposure to a natural oceanic environment. Caution is in order because, based on past experience of underwater research at NUWC, in some cases extrapolation of developments from clean water to oceanic environments can be fatal.

By many accounts, the NUWC flapping fin propulsion and control technology has matured. These technologies have been built in *affordable* modular form that is detachable/attachable to a platform. Future prospects include their evaluation for stabilizing (and recovering) platforms in distress and in high sea states, or for tautening towed cables. Future interest in biorobotics would be sustained if its mission value is continuously demonstrated to the users and if it is combined with conventional approaches. In basic research, an assessment needs to be made to identify the nagging obstacles to the development of strong muscle technology. In biorobotics basic research, integration of the SPR mechanism with flapping fins needs to be generalized. The results in Figs. 11.2 through 11.7 indicate that in the current stage of maturity, biorobotics is straddling between the laboratory and near-shore open waters.

11.7 Concluding Remarks

UUVs have wide-ranging naval utility. They are the main work horse for unmanned missions, and their long range, versatile payload capacity, and operational envelope offer advantage and value in many naval applications. However, our studies have documented that a large gap in turning ability exists between fish and tactical scale UUVs [11.50]. Advances in digital control have not been able to close this gap. As a result, the gap has been attributed to differences in the hydrodynamic mechanism of lift production – lift production in steady fins versus that in flapping fins – that is, attached fin flow versus pinned-LEV type modified dynamic stall. At NUWC, we have proceeded to implement the high-lift mechanism of flapping fins to naval utility in hovering and low-speed maneuvering, while others have proceeded to mimic swimming animals. These approaches to the development of biology-inspired UUVs have been reviewed by filtering those that we believe have matured the most.

The low-aspect-ratio, rigid flapping fin has been found to be the most successful actuator in the biology-inspired UUVs. We have also been able to mate the flapping fins to rigid cylinders – the most widely used underwater hull form, and also to noncylindrical sections.

Maneuverability and controllability have been demonstrated in both bio-inspired and bio-mimicry

UUVs. Mission concepts, duration, payload capabilities, and sensor integration have been demonstrated, and the former type of UUV appears to be somewhat more advanced than the latter. A six-finned cylindrical UUV has demonstrated long-duration reliability, performing incessant swimming for nearly 3 weeks with low power consumption (Fig. 11.7).

While conventional PID controllers have been successfully developed for use with flapping fins, which produce oscillatory forces, control of the instantaneous unsteady forces due to flapping fins using olivocerebellar dynamics should make the UUVs more animal-like [11.24–26, 33, 51, 52]. This would give a more logical foundation to the integration of nonlinear sensors and would also make the UUV controller robust and most responsive to unsteady environmental disturbances. Autonomy is theoretically described as a consequence of the self-regulating property of nonlinear oscillators.

To date, significant progress has been lacking in the development of strong artificial muscles [11.44, 47, 48, 53, 54] and nonlinear sensing [11.35] for underwater application. When these developments move forward, their integration with flapping fins controlled by olivocerebellar dynamics would lead to radically new naval precision and other capabilities.

11.8 Nomenclature

A	Amplitude of fin oscillation	U, U_{wing}, U_t	Cruise speed, wing speed, and total forward speed
$C_{x,\text{wing}}$	Coefficient of axial thrust in a single flapping fin [11.15]	u_i, v_i, z_i, w_i	States of oscillator i
F	Cubic polynomial function	α	Effective fin angle of attack considering fin–wake coupling
F'_x, F'_{x0}	Instantaneous fluctuating force and force amplitude, respectively	α_g	Geometric fin angle of attack (excluding fin–wake coupling)
f, ω, ω_s	Frequency of fin oscillation	Γ_i	Limit cycle orbit
G, T	Constants	$\varepsilon_{\text{Ca}}, \varepsilon_{\text{Na}}$	Factors controlling oscillator time scale of oscillation of inferior-olive neuron
$I_{\text{Ca}}, I_{\text{Na}}$	Factors driving depolarization level of inferior-olive neuron	$\theta(t), \theta_0, \theta_{\text{Bias}}$	Pitch at time t , pitch amplitude, and pitch bias angle, respectively
$I_{\text{exti}}(t)$	External stimulus	$\xi(t)$	Combined roll and pitch angle
k	Factor that sets a relative time scale between the uv - and zw -subsystems	$\tau_w(t)$	Temporal local wall-shear stress on the flapping fin surface
p_{iu}, p_{iz}	Nonlinear functions of u_i and z_i , respectively	$\phi(t), \phi_0$	Roll angle at time t and roll amplitude, respectively
R_{avg}	Average fin radius	ψ	Phase difference between roll and pitch oscillations
Re_c	Fin chord (c) Reynolds number Uc/ν		
St	Strouhal number of a flapping fin, $\text{St} = \frac{2f\phi_0 R_{\text{avg}}}{U}$		

References

- 11.1 T. von Karman, J.M. Burgers: *General Aerodynamic Theory: Perfect Fluids*, Aerodynamic Theory, Vol. II (Springer, Leipzig 1934), ed. by W. F. Durand
- 11.2 J. Lighthill: *Mathematical Biofluidynamics*, CBMS-NSF Regional Conference Series in Applied Mathematics (IAM, Philadelphia 1975)
- 11.3 P.R. Bandyopadhyay, H.A. Leinhos: Propulsion efficiency of bodies appended with multiple flapping fins: When more is less, *Phys. Fluids* **25**(4), 041902 (2013)
- 11.4 P.R. Bandyopadhyay, M. Boller: Convergence in underwater swimming between nature and engineering, Proc. 14th Unmanned Untethered Submers. Technol. (2005)
- 11.5 S. Saunders (Ed.): *Jane's Fighting Ships 2004–2005* (Janes Information Group, Coulsdon 2004)
- 11.6 T. Hooton (Ed.): *Jane's Naval Weapon Systems* (Janes Information Group, Coulsdon 2005)
- 11.7 P.R. Bandyopadhyay: Trends in biorobotic autonomous undersea vehicles, *IEEE-JOE* **30**(1), 109–139 (2005)
- 11.8 T.M. McKenna: Commentary: Developing bio-inspired autonomous systems, *Marine Tech. Soc. J.* **45**(4), 19–23 (2011)
- 11.9 P.R. Bandyopadhyay: Review: Swimming and flying in nature – the route toward applications: The Freeman scholar lecture, *ASME J. Fluids Eng.* **129**, 31801–31829 (2009)
- 11.10 P.R. Bandyopadhyay: Biology-inspired science and technology for autonomous underwater vehicles, *IEEE-JOE* **29**(3), 542–806 (2004)
- 11.11 M.S. Triantafyllou, A.H. Techet, F.S. Hover: Review of experimental work on biomimetic foils, *IEEE-JOE* **29**, 585–594 (2004)
- 11.12 M.S. Triantafyllou, F.S. Hover, A.H. Techet, D.K.P. Yue: Review of hydrodynamic scaling laws in aquatic locomotion and fishlike swimming, *Appl. Mech. Rev.* **58**, 226–237 (2005)
- 11.13 M. Sfakiotakis, D.N. Lame, J.V.C. Davis: 1999 Review of fish swimming modes for aquatic locomotion, *IEEE-JOE* **24**(2), 237–252 (1999)
- 11.14 P.R. Bandyopadhyay, H.A. Leinhos, J.D. Hrubes, N. Toplosky, J.C. Hansen: Turning of a short-length cable using flapping fin propulsion, *IEEE-JOE* **36**(4), 571–585 (2011)
- 11.15 P.R. Bandyopadhyay, D.N. Beal, J.D. Hrubes, A. Mangalam: Relationship of roll and pitch oscillations in a fin of low aspect ratio and rounded leading edge flapping at transitional to high Reynolds numbers, *J. Fluid Mech.* **702**, 298–331 (2012)
- 11.16 P.R. Bandyopadhyay, D.N. Beal, A. Menozzi: Biorobotic insights into how animals swim, *J. Exp. Biol.* **211**, 206–214 (2008)
- 11.17 D.N. Beal, P.R. Bandyopadhyay: Comparison of steady-state and unsteady hydrodynamic mechanisms, Proc. 14th Unmanned Untethered Submers. Technol. (2005)
- 11.18 G.V. Lauder, E.G. Drucker: Morphology and experimental hydrodynamics of fish fin control surfaces, *IEEE-JOE* **29**(3), 556–571 (2004)
- 11.19 A. Menozzi, H.A. Leinhos, D.N. Beal, P.R. Bandyopadhyay: Open-loop control of a multi-fin biorobotic underwater vehicle, *IEEE-JOE* **33**(2), 59–68 (2008)
- 11.20 J. Walker: Kinematics and performance of maneuvering control surfaces in teleost fishes, *IEEE-JOE* **29**(3), 572–584 (2004)
- 11.21 M. Rufo, M. Smithers: Ghostswimmer AUV: Applying biomimetics to underwater robotics for achievement of tactical relevance, *Marine Tech Soc. J.* **45**(4), 24–30 (2011)
- 11.22 J. Piotrowski: A Fin-tuned Design, http://www.economist.com/node/12494717?story_id=12494717 (2008), *The Economist*
- 11.23 M. S. Triantafyllou: D. Isla robotuna project to model real fish, *The Tech Online Edition*, **115**(115), (1995), <http://tech.mit.edu/V115/N49/robotuna.49n.html>, also <https://en.wikipedia.org/RoboTuna>
- 11.24 R.R. Llinas, Y. Yarom: Electrophysiology of mammalian inferior-olive neurons in vitro, different types of voltage dependences in conductances, *J. Physiol.* **315**, 549–567 (1981)
- 11.25 R.R. Llinas: *I of the Vortex* (MIT Press, Cambridge 2001)
- 11.26 V.B. Kazantsev, V.I. Nekorkin, V.I. Makarenko, R. Llinas: Olivo-cerebellar cluster-based universal control system, *Proc. Nat. Acad. Sci.* **100**(22), 13064–13068 (2003)
- 11.27 R.R. Llinas, E. Leznik, V.I. Makarenko: The olivo-cerebellar circuit as a universal control system, *IEEE-JOE* **29**(3), 631–639 (2004)
- 11.28 P.R. Bandyopadhyay, H.A. Leinhos, A.M. Hellum: Handedness helps homing in swimming and flying animals, *Sci. Rep.* **3**, 1128 (2013)
- 11.29 N. Vandenberghe, N.J. Zhang, S. Childress: Symmetry breaking leads to forward flapping flight, *J. Fluid Mech.* **506**, 147–155 (2004)
- 11.30 D. Lentink, M.H. Dickinson: Rotational accelerations stabilize leading edge vortices on revolving fly wings, *J. Exp. Biol.* **212**, 2705–2719 (2009)
- 11.31 P. Albarède, P.A. Monkewitz: A model for the formation of oblique shedding and Chevron patterns in cylinder wakes, *Phys. Fluids A* **4**, 74–756 (1992)
- 11.32 R.A. Skop, S. Balasubramanian: A new twist on an old model for vortex-induced vibrations, *J. Fluids Struct.* **11**, 39–412 (1997)
- 11.33 P.R. Bandyopadhyay, S.N. Singh, D.P. Thivierge, A.M. Annaswamy, H.A. Leinhos, A.R. Fredette, D.N. Beal: Synchronization of animal-inspired multiple fins in an underwater vehicle using olivo-cerebellar dynamics, *IEEE-JOE* **33**(4), 563–578 (2008)
- 11.34 H.K. Khalil: *Nonlinear Systems* (Prentice Hall, Upper-Saddle River 1996)
- 11.35 P.R. Bandyopadhyay, J.C. Hansen: Breakup and then makeup: A predictive model of how cilia self-regulate their hardness for posture control, *Sci. Rep.* **3**, 1956 (2013)
- 11.36 S. Forsythe, H.A. Leinhos, P.R. Bandyopadhyay: Dolphin-inspired maneuvering and pinging for

- short distance echolocation, *J. Acous. Soc. Am. Express Lett.* **124**, EL255–EL261 (2008)
- 11.37 R. Berube: H. Leinhos, personal communication (2011)
- 11.38 Autonomous Undersea Vehicles Application Center: AUV System Spec Sheet RAZOR Configuration, <http://auvac.org/configurations/view/218> (2015)
- 11.39 S.C. Licht: Biomimetic Oscillating Foil Propulsion to Enhance Underwater Vehicle Agility and Maneuverability, Ph.D. Thesis (MIT, Cambridge 2008)
- 11.40 P.R. Bandyopadhyay: A novel large slosh-or-spin low speed underwater propulsor bridges the unsteady and steady propulsion mechanisms of nature and engineering, *IEEE-JOE* (2016), doi:10.1109/JOE.2015.2497879
- 11.41 D.P. Thivierge, P.R. Bandyopadhyay: Power conditioner for microbial fuel cells, US Patent 8232761 (2012)
- 11.42 P.R. Bandyopadhyay, D.P. Thivierge, F.M. McNeilly, A. Fredette: An electronic circuit for trickle charge harvesting and its evaluation in littoral basin, *IEEE-JOE* **38**(1), 32–42 (2013)
- 11.43 P.R. Bandyopadhyay, J.D. Hrubes, H.A. Leinhos: Biorobotic adhesion in water using suction cups, *Inst. Phys. J. Bioinspiration Biomim.* **3**, 016003 (2008)
- 11.44 P.R. Bandyopadhyay: Emerging approaches to flow control in hydrodynamics, *Proc. 38th IEEE CDC'99* (1999) pp. 2845–2850
- 11.45 P.R. Bandyopadhyay, W.P. Krol, D.P. Thivierge, W.H. Nedderman, M.A. Mojarrad: *Biomimetic Propulsor for Active Noise Control: Experiments*, NUWC Techn. Rep. 11351 (Naval Undersea Warfare Center, Newport 2002)
- 11.46 W.P. Krol, A. Annaswamy, P.R. Bandyopadhyay: A Biomimetic Propulsor for Active Noise Control, NUWC Techn. Rep. 11350 (Naval Undersea Warfare Center, Newport 2002)
- 11.47 P.G.A. Madden, J.D.W. Madden, P.A. Anquetil, N.A. Vandesteeg, I. Hunter: The relation of conducting polymer actuator material properties to performance, *IEEE-JOE* **33**(3), 696–705 (2004)
- 11.48 J.D.W. Madden, N.A. Vandesteeg, P.A. Anquetil, P.G.A. Madden, A. Takshi, R.Z. Pytel, S.R. LaFontaine, P.A. Wieringa, I. Hunter: Artificial muscle technology: Physical principles and naval properties, *IEEE-JOE* **33**(3), 706–728 (2004)
- 11.49 I.K. Bartol, R. Mann, M.R. Patterson: Aerobic respiratory costs of swimming in the negatively buoyant brief squid *Lolliguncula brevis*, *J. Exp. Biol.* **204**, 3639–3653 (2001)
- 11.50 P.R. Bandyopadhyay: Maneuvering hydrodynamics of fish and small underwater vehicles, *J. Integ. Comp. Biol.* **42**(1), 102–117 (2002)
- 11.51 A. Menozzi, P.R. Bandyopadhyay, S. Warren: Interfacing olivo-cerebellar neuron hardware to fin actuators of a biorobotic autonomous underwater vehicle, *Proc. IASTED Conf. Intell. Syst. Control* (2005), Paper No. 497–104
- 11.52 P.R. Bandyopadhyay, A. Menozzi, D.P. Thivierge, D.N. Beal, A. Annaswamy: Auto-catalytic oscillators for locomotion of underwater vehicles, US Patent 7869910 (2011)
- 11.53 J.W. Paquette, K. Kim: Ionomeric electroactive polymer artificial muscle for naval applications, *IEEE-JOE* **33**(3), 729–737 (2004)
- 11.54 K.J. Kim, X. Tan, H.R. Choi, D. Pugal: *Biomimetic Robotic Artificial Muscles* (World Scientific, Hackensack 2013)